Crystal structure effect on the ferromagnetic correlations in ZnO with magnetic impurities

Bo Gu,[1,a)] Nejat Bulut,[1,2] and Sadamichi Maekawa[1,2]
[1]*Institute for Materials Research, Tohoku University, Sendai 980-8577, Japan*
[2]*JST, CREST, 3-Sanbancho, Chiyoda-ku, Tokyo 102-0075, Japan*

(Received 24 July 2008; accepted 8 October 2008; published online 18 November 2008)

We study the ferromagnetism in the compound (Zn,Mn)O within the Haldane–Anderson impurity model by using the quantum Monte Carlo technique and the tight-binding approximation for determining the host band structure and the impurity-host hybridization. This computational approach allows us to determine how the host crystal structure influences the impurity bound state, which plays an important role in the development of the ferromagnetic (FM) correlations between the impurities. We find that the FM correlations are strongly influenced by the crystal structure. In particular, in *p*-type (Zn,Mn)O, we observe the development of FM correlations with an extended range at low temperatures for wurtzite and zinc-blende crystal structures. However, for the rocksalt structure, no FM correlations are observed between the impurities. In addition, in *n*-type ZnO with magnetic impurities, the impurity bound state and FM correlations are not found. © *2008 American Institute of Physics*. [DOI: 10.1063/1.3028262]

I. INTRODUCTION

Dilute magnetic semiconductors (DMSs) could lead to new spintronic devices where both the electronic charge and spin can be controlled. For practical applications, DMS with Curie temperature T_C above room temperature are required. The (Ga,Mn)As is regarded as a classic example with robust ferromagnetism,[1] but the highest reported T_C's are still well below room temperature.[2,3] Alternatively, *p*-type (Zn,Mn)O has been predicted to be a room-temperature ferromagnet,[4,5] where ferromagnetism above room temperature has been observed for Mn doped pure ZnO (Ref. 6–9) or Mn doped *p*-type ZnO.[10–15] However, contradictory experimental results have also been reported for (Zn,Mn)O such as ferromagnetism below room temperature,[16] absence of ferromagnetism,[17] spin glass behavior,[18] or paramagnetism.[19,20]

The possibility of room-temperature ferromagnetism motivates the theoretical research on the origin and control of high-temperature ferromagnetism in semiconductors, especially ZnO-based DMS, which is the subject of this paper. Magnetic impurities in ordinary metals exhibit the well-known Ruderman–Kittel–Kasuya–Yosida oscillations, which is a carrier mediated indirect coupling due to the Friedel oscillations of the polarized carriers around the impurities. When magnetic impurities are doped into a semiconductor host, quite different behaviors are experimentally observed as mentioned above. The Haldane–Anderson impurity model had been introduced to study transition-metal impurities in semiconductors.[21] After the discovery of DMS, the magnetic properties of this model were addressed within the Hartree–Fock (HF) approximation,[22] and it was shown that long-range ferromagnetic (FM) correlations develop when the Fermi level is located between the top of the valence band and the impurity bound state (IBS). The FM interaction between the impurities is mediated by the impurity-induced polarization of the valence electron spins, which exhibit an antiferromagnetic coupling to the impurity moments. Subsequent quantum Monte Carlo (QMC) calculations[23] on the two-impurity Haldane–Anderson model with the Hirsch–Fye algorithm have supported this picture for the generation of FM correlations between magnetic impurities in semiconductors. Various other theoretical approaches have also been used to study magnetic impurities in semiconductors. The Zener model has been invoked to describe the ferromagnetism in semiconductors.[4] Numerical calculations based on local spin density approximation have also found that magnetic states and corresponding Curie temperatures in ZnO-based DMS are controlled by changing the carrier density or the magnetic impurity concentration.[5,24–27] Within the context of DMS, the Anderson Hamiltonian for a semiconductor host was also considered by Krstajić *et al.*,[28] and it was shown that an FM interaction is generated between the impurities due to kinematic exchange. The role of IBS in producing the FM interaction in DMS was also discussed within the "double resonance mechanism" using HF.[29]

In this paper, we present QMC results for the compound (Zn,Mn)O. For ZnO host, the wurtzite structure is the most common phase, and thus almost all experiments for ZnO are focused on this structure. However, ZnO with the zinc-blende and the rocksalt structures are also experimentally possible in thin films and at high pressure, respectively.[30] The band structures of ZnO with the wurtzite, zinc-blende, and rocksalt structures had been already calculated within a single set of tight-binding parameters,[30] and we will follow these results in this paper to study the ferromagnetism for the compound (Zn,Mn)O with experimentally determined values for the *p-d* mixing and the onsite Coulomb repulsion.[31] For the doped Mn^{2+} impurity, we neglect the Hund coupling among the five occupied 3*d* orbitals, and, for simplicity, consider the 3*d* orbitals independently. In the dilute impurity limit, the Haldane–Anderson impurity model is invoked to

[a)]Electronic mail: bogu@imr.tohoku.ac.jp.

describe the magnetic states of Mn^{2+} ions. The results of the numerical calculations show that the crystal structure of the ZnO host strongly influences the energy of the IBS and the strength of the magnetic correlations between the impurities. In particular, for the wurtzite and zinc-blende structures, we find that FM correlations with an extended range develop at low temperatures. However, for the rocksalt structure, FM correlations have not been observed because, in this case, the IBS is located at much higher frequencies. In addition, only *p*-type (Zn,Mn)O is found to exhibit FM correlations.

To yield accurate predictions about ferromagnetism in DMS materials, we think that the combining the band-calculation and QMC techniques is the first and crucial approach, in which the strong electron correlation is exactly taken into account. In this paper, we combine the tight-binding calculations for the host band structure and the impurity-host hybridization with the QMC simulations. Our purpose in this paper is to investigate the effect of the crystal structure of the semiconductor host on the FM correlations between the impurities, so the Haldane–Anderson model, which considers one of five *d* orbitals, is reasonably enough to explore the main properties of this effect. For the multiorbital effect, where all five of the impurity $3d$ orbitals are included with the Hund couplings, is another quite different effect, and thus ignored in this paper.

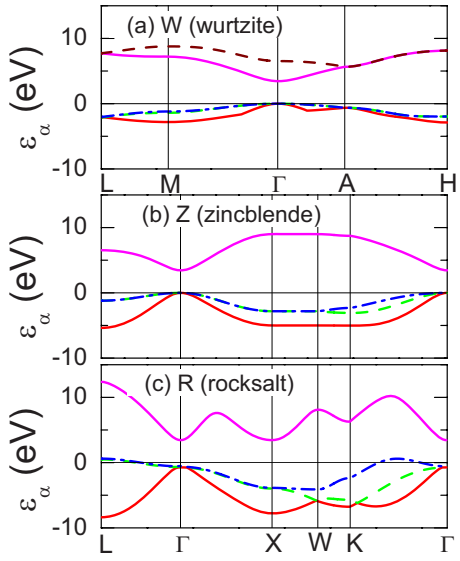

FIG. 1. (Color online) Energy bands of the ZnO host near the semiconductor gap with (a) wurtzite, (b) zinc-blende, and (c) rocksalt crystal structures obtained using the tight-binding approximation. These results were reproduced using the parameters given in Ref. 30.

II. IMPURITY MODEL

In order to describe the transition-metal impurities in a ZnO host, we use the Haldane–Anderson impurity model,[21] which is defined by

$$H = \sum_{\mathbf{k},\alpha,\sigma} [\epsilon_\alpha(\mathbf{k}) - \mu] c^\dagger_{\mathbf{k}\alpha\sigma} c_{\mathbf{k}\alpha\sigma} + \sum_{\mathbf{k},\alpha,\mathbf{i},\xi,\sigma} (V_{\mathbf{i}\xi\mathbf{k}\alpha} d^\dagger_{\mathbf{i}\xi\sigma} c_{\mathbf{k}\alpha\sigma} + Hc) + (E_d - \mu) \sum_{\mathbf{i},\xi,\sigma} d^\dagger_{\mathbf{i}\xi\sigma} d_{\mathbf{i}\xi\sigma} + U \sum_{\mathbf{i},\xi} n^\dagger_{\mathbf{i}\xi\uparrow} n_{\mathbf{i}\xi\downarrow}, \quad (1)$$

where $c^\dagger_{\mathbf{k}\alpha\sigma}$ ($c_{\mathbf{k}\alpha\sigma}$) is the creation (annihilation) operator for a host electron with wavevector $\mathbf{k}$ and spin σ in the valence ($\alpha=v$) or conduction ($\alpha=c$) band and $d^\dagger_{\mathbf{i}\xi\sigma}$ ($d_{\mathbf{i}\xi\sigma}$) is the creation (annihilation) operator for a localized electron at impurity site $\mathbf{i}$ in orbital ξ and spin σ with $n_{\mathbf{i}\xi\sigma}=d^\dagger_{\mathbf{i}\xi\sigma}d_{\mathbf{i}\xi\sigma}$. Here, $\epsilon_\alpha(\mathbf{k})$ is the host band dispersion, μ is the chemical potential, $V_{\mathbf{i}\xi\mathbf{k}\alpha}$ is the mixing between the impurity and host, E_d is the impurity ξ-level energy, and U is the onsite Coulomb repulsion for the impurity.

The energy bands $\epsilon_\alpha(\mathbf{k})$ and the impurity-host hybridization $V_{\mathbf{i}\xi\mathbf{k}\alpha}$ will be calculated within the tight-binding approximation for the wurtzite, zinc-blende, and rocksalt crystal structures of the ZnO host material. For the compound (Zn,Mn)O, the value of the onsite Coulomb repulsion for Mn^{2+} is taken as $U=5.2$ eV by comparing with the photoemission spectroscopy measurements.[31] In addition, because the experimental value of E_d for Mn^{2+} in ZnO host is unknown, in the following, we use $E_d=\mu-U/2$ so that the impurity sites develop large magnetic moments. The results on the magnetic correlations between the impurities depend weakly on small variations on the value of E_d.

III. TIGHT-BINDING APPROACH FOR THE ZNO BAND STRUCTURE AND THE IMPURITY-HOST HYBRIDIZATION

In this section, we discuss the tight-binding calculation of the band structure of the ZnO host, and the impurity-host hybridization. The energy bands $\epsilon_\alpha(\mathbf{k})$ of ZnO had been already calculated for the wurtzite, zinc-blende, and rocksalt structures using a single set of sp^3 tight-binding parameters.[30] In this approach, the basis consists of one $4s$ and three $4p$ orbitals for cation Zn^{2+} and three $2p$ orbitals for anion O^{2-}. The values of the orbital energies are $E_p(\mathrm{O})=0.550$ eV, $E_s(\mathrm{Zn})=3.450$ eV, and $E_p(\mathrm{Zn})=13.050$ eV. In addition, the mixing values between the *s* and *p* orbitals of Zn^{2+} and the *p* orbitals of O^{2-} are taken to be $(sp\sigma)=2.965$ eV, $(pp\sigma)=4.324$ eV, and $(pp\pi)=-1.157$ eV.

Using these tight-binding parameters and keeping all of the branches within the sp^3 basis, we have reproduced the band structure of ZnO. In Figs. 1(a)–1(c), we have plotted the branches near the semiconductor gap. Here, we observe that for the wurtzite and zinc-blende structures, the top of the valence band is located at the Γ point with a direct gap of 3.45 eV. For the rocksalt case, the top of the valence band, located at the *L* point, is at 0.6 eV, while the Γ point is at −0.53 eV. Hence, for the rocksalt structure, the system has an indirect semiconductor gap.

Next, we discuss the calculation of the impurity-host hybridization within the tight-binding approximation. Once a substitutional impurity Mn^{2+} is introduced and takes the position of a Zn^{2+} cation, the $3d$ orbital ξ of Mn^{2+} will mix with the neighboring $2p$ orbitals of O^{2-}. The mixing matrix element $V_{\mathbf{i}\xi\mathbf{k}\alpha} \equiv \langle \varphi_\xi(\mathbf{i}) | H | \Psi_\alpha(\mathbf{k}) \rangle$ has the form of

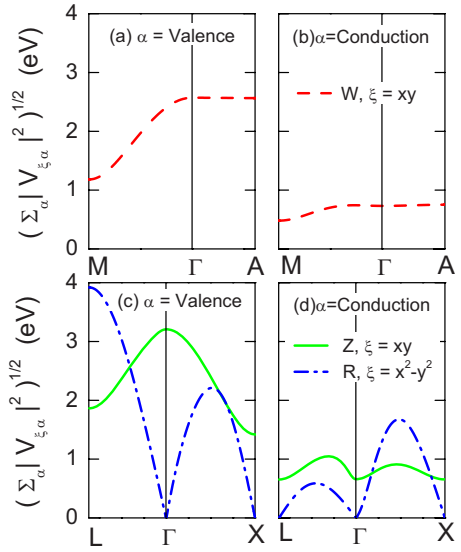

FIG. 2. (Color online) Hybridization function $\bar{V}_{\xi}(\mathbf{k})$ of a single Mn^{2+} orbital with the valence bands [(a) and (c)] or the conduction bands [(b) and (d)]. Here, results are shown for a Mn^{2+} $3d(xy)$ orbital in the wurtzite or zinc-blende ZnO and for a Mn^{2+} $3d(x^2-y^2)$ orbital in the rocksalt ZnO. In obtaining these results, we have used mixing parameters with values taken from Ref. 31.

$$V_{\mathbf{i}\xi\mathbf{k}\alpha} = \frac{1}{\sqrt{N}} e^{i\mathbf{k}\cdot\mathbf{i}} \sum_{p,\mathbf{n}} e^{i\mathbf{k}\cdot(\mathbf{n}-\mathbf{i})} a_{\alpha p}(\mathbf{k}) \langle \varphi_{\xi}(\mathbf{i}) | H | \varphi_{p}(\mathbf{n}) \rangle$$

$$\equiv \frac{1}{\sqrt{N}} e^{i\mathbf{k}\cdot\mathbf{i}} V_{\xi\alpha}(\mathbf{k}), \tag{2}$$

where $\varphi_{\xi}(\mathbf{i})$ is the impurity $3d$-state at site $\mathbf{i}$ and $\Psi_{\alpha}(\mathbf{k})$ is the host state with wavevector $\mathbf{k}$ and band index α, which is expanded by atomic orbitals $\varphi_{p}(\mathbf{n})$ with orbital index p and site index $\mathbf{n}$. Here, N is the total number of host lattice sites and $a_{\alpha p}(\mathbf{k})$ is an expansion coefficient. For the p-d mixing integrals of $\langle \varphi_{\xi}(\mathbf{i}) | H | \varphi_{p}(\mathbf{n}) \rangle$, p represents the three $2p$ orbitals of O^{2-} and ξ denotes the five $3d$ orbitals of Mn^{2+}. As shown by Slater and Koster,[32] these 15 mixing integrals can be expressed by only two integrals $(pd\sigma)$ and $(pd\pi)$ and direction cosines l, m, and n in the two-center approximation. In this approach, the integrals $(pd\sigma)$ and $(pd\pi)$ are taken as fitting parameters, which can then be determined by other exact results or by comparison with the experimental data. For the compound (Zn,Mn)O, the value of $(pd\sigma)=-1.6$ eV has been estimated by comparing with the photoemission spectroscopy measurements,[31] while the value of $(pd\pi)$ is always determined by the relation $(pd\pi)=-(pd\sigma)/2.16$.[33] We will use these values in the rest of this paper.

It is established that for the wurtzite or zinc-blende crystal structures, the p-d mixing is dominated by the occupied t_{2g} (xy, yz, zx) orbitals because of the tetrahedral crystal field, while for the rocksalt structure, the p-d mixing comes mainly from the occupied e_g (x^2-y^2, z^2) orbitals due to the octahedral crystal field.[34] For simplicity, here we consider only one of the t_{2g} orbitals ($\xi=xy$ orbital here) for the (Zn,Mn)O with wurtzite and zinc-blende structures and only one of the e_g orbitals ($\xi=x^2-y^2$ orbital here) for the (Zn,Mn)O with rocksalt structure.

Figure 2 displays results on the p-d mixing function $\bar{V}_{\xi}(\mathbf{k})$ defined by

$$\bar{V}_{\xi}(\mathbf{k}) \equiv \left(\sum_{\alpha} |V_{\xi\alpha}(\mathbf{k})|^2 \right)^{1/2}, \tag{3}$$

where only one of the Mn^{2+} $3d$ orbitals, labeled by ξ, is considered. In Eq. (3), the summation over α is performed only over the valence bands [Figs. 2(a) and 2(c)] or the conduction bands [Figs. 2(b) and 2(d)]. Here, $\bar{V}_{\xi}(\mathbf{k})$ is plotted along various cuts in the Brillouin zone for wurtzite, zinc-blende, and rocksalt crystal structures. Figures 2(a) and 2(b) show $\bar{V}$ for a Mn $3d(xy)$ orbital when the ZnO has the wurtzite structure. Here, we observe that at the Γ point, the total hybridization of the xy orbital with the valence bands is about three times larger than that with the conduction bands. For the wurtzite and the zinc-blende structures, the semiconductor gap edges are located at the Γ point, hence, the value of $\bar{V}$ near Γ will be particularly important in determining the energy of the IBS and the strength of the magnetic correlations between the impurities. Figures 2(c) and 2(d) show that for the case of a Mn $3d(xy)$ orbital in ZnO with the zinc-blende structure, the total hybridization with the valence bands is also stronger than that with the conduction bands near the Γ point. Figures 2(c) and 2(d) also show results for a Mn $3d(x^2-y^2)$ orbital in the rocksalt structure. Here, we see that the total hybridization with the valence and the conduction bands vanish at the Γ point. However, at the L point, where the top of the valence band is located, the total hybridization with the valence band is the stronger than in the rest of the cases.

The results on the frequency of the IBS and the strength of the FM correlations depend sensitively on the value of hybridization near the gap edges, which we will discuss in the next section. We note that in turn, the hybridization depends strongly on the values of the mixing parameters $(pd\sigma)$ and $(pd\pi)$ of the tight-binding approach.

IV. QUANTUM MONTE CARLO RESULTS

In this section, we present results on the impurity magnetic correlations, which were obtained using the Hirsch–Fye QMC technique.[35] The input parameters for the QMC simulations were calculated with the tight-binding approach described above. The following results were obtained with more than 10^5 Monte Carlo sweeps and Matsubara time step $\Delta\tau=0.225$.

We first discuss the local moment formation at an impurity orbital. For this purpose, we have performed QMC simulations to calculate $\langle (M^z)^2 \rangle$, where

$$M^z = n_{\mathbf{i}\xi\uparrow} - n_{\mathbf{i}\xi\downarrow} \tag{4}$$

is the magnetization operator for a single $3d(\xi)$ orbital at the impurity site $\mathbf{i}$. We have performed the calculations for a single $3d$ orbital because in this paper we are mainly interested in the effects of the host crystal and we neglect the multiorbital effects, which we will treat in a separate paper. Hence, $\langle (M^z)^2 \rangle$ represents the square of the local-moment for a single $3d$ orbital added to the ZnO host.

Figures 3(a) and 3(b) show results on $\langle (M^z)^2 \rangle$ for a $3d(xy)$ orbital in wurtzite and zinc-blende structures and a

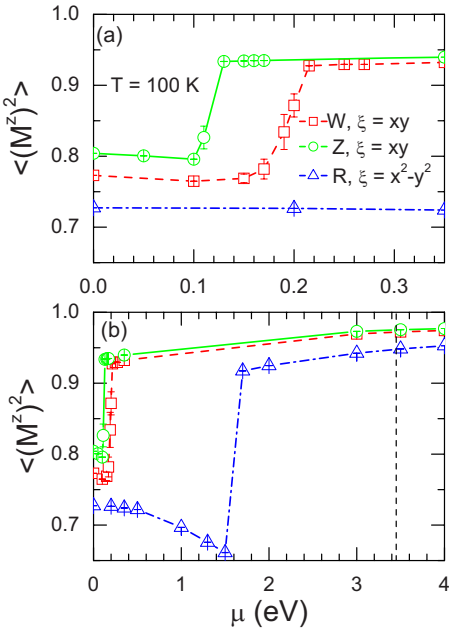

FIG. 3. (Color online) Square of the magnetic moment at the impurity site $\langle (M^z)^2 \rangle$ vs the chemical potential μ for different energy intervals at $T=100$ K. These results were obtained for a single Mn^{2+} $3d(\xi)$ orbital added to the ZnO host. For the wurtzite and zinc-blende crystal structures, we have considered a $\xi=xy$ orbital, while for the rocksalt case an x^2-y^2 orbital. The vertical dashed line denotes the bottom of the conduction band.

$3d(x^2-y^2)$ orbital in the rocksalt ZnO. In Fig. 3(a), $\langle (M^z)^2 \rangle$ versus the chemical potential μ is plotted for 0 eV$<\mu<$0.35 eV and in Fig. 3(b) for 0 eV$<\mu<$4 eV. These results are for temperature $T=100$ K. In these figures, we observe discontinuities at 0.12, 0.20, and 1.6 eV for the zinc-blende, wurtzite, and rocksalt structures, respectively.

According to the HF and QMC calculations, the presence of a discontinuity in $\langle (M^z)^2 \rangle$ versus μ implies the existence of an IBS at this energy.[22,23] A step discontinuity develops in the magnitude of the magnetic moment as μ increases through ω_{IBS} because impurity spectral weight is induced in the semiconductor gap at ω_{IBS} for sufficiently strong hybridization. When the IBS is occupied, the spin polarization of the host split-off state, which is due to the impurity-host mixing and at the same energy as the IBS, will cancel the spin polarization of the valence band. Thus antiferromagnetic couplings between the polarized host carriers and the impurities disappear. This causes the FM interaction between the impurities, which is mediated by the polarized carriers around the magnetic impurities, to vanish. In this paper, we are studying how this mechanism of FM correlations is influenced by the crystal structure of the ZnO host. The variation in the values of ω_{IBS} for different crystal structures seen in Fig. 3 is clearly a consequence of the differences in the energy bands and the impurity-host mixing. In addition, the values of the hybridization with the bottom of the conduction bands are weaker, and hence we do not observe bound states near the bottom of the conduction band.

The value of ω_{IBS} plays an important role in determining the strength of the FM correlations which develop between the impurities when the IBS is unoccupied. Within the HF approximation and for a semiconductor host with constant density of states ρ_0 and semi-infinite bands,[22] the range of the FM correlations between the impurities is given by

$$\ell_0 \approx \frac{1}{\sqrt{16\pi\rho_0\omega_{\mathrm{IBS}}}}, \tag{5}$$

when the IBS is unoccupied ($0<\mu<\omega_{\mathrm{IBS}}$). However, when the IBS becomes occupied ($\omega_{\mathrm{IBS}}<\mu$), the FM correlations become weaker. The QMC calculations performed for a two-dimensional (2D) semiconductor host with quadratic quasiparticle dispersion confirm this picture.[23] These QMC calculations show that in 2D, ω_{IBS} increases as the strength of the hybridization grows. The maximum range of the FM correlations decreases as ω_{IBS} increases in agreement with the HF calculations. However, in the three-dimensional case, the IBS does not exist if the hybridization is smaller than a critical value.[36]

In the following calculations, we will see that the magnetic correlations between the impurities are sensitive to the location of the chemical potential with respect to the IBS. An IBS with shallower position ($\omega^Z_{\mathrm{IBS}} \approx 0.1$ eV) is obtained for (Zn,Mn)O with the zinblende structure, while a much deeper IBS ($\omega^R_{\mathrm{IBS}} \approx 1.6$ eV) is found for the rocksalt case. Based on the previous HF and QMC calculations,[22,23] it is reasonable to expect that the FM correlation range for (Zn,Mn)O with the wurtzite structure will be shorter than that with the zinc-blende structure and will be much longer than that of the rocksalt case.

In addition, it should be pointed out that the IBS for (Zn,Mn)O with wurtzite and zinc-blende structures only exists near the top of valence band, while no IBS is found near the bottom of conduction band. If instead of Mn^{2+} another transition metal ion TM^{2+} is substituted into the ZnO host, then the only different quantities would be the p-d mixing parameters $(pd\sigma)$ and $(pd\pi)$ within this framework. In particular, for various hosts and transition-metal impurities, the p-d mixing parameters, which are consistent with the experimental measurements, are mostly in the range -1.6 eV $\leq (pd\sigma) \leq -1.0$ eV,[31,37] while $(pd\pi)=-(pd\sigma)/2.16$.[33] We have checked the IBS for (Zn,TM)O for various p-d mixing values in the above mentioned range. We find that when smaller values are used for the p-d mixing, the IBS shifts toward the top of valence band, while at the same time no IBS develops near the bottom of the conduction band. Since the doping of the transition metal ion TM^{2+} into the ZnO host does not itself introduce carriers, the hole and electron carriers in (Zn,TM)O are associated with *additional* the acceptor or donor defects, respectively. This implies that for p-type (Zn,TM)O, the FM correlations will develop when $0 \leq \mu \leq \omega_{\mathrm{IBS}}$, while for the n-type (Zn,TM)O, no FM correlations are expected due to the absence of the IBS. In fact, the existence of p-type rather than n-type (Zn,Mn)O with wurtzite structure has recently been pointed out based on the analysis of the experimental measurements.[13,14]

We next display results on the impurity-impurity magnetic correlation function $\langle M^z_1 M^z_2 \rangle$ versus the impurity separation R/a in Fig. 4. These results are for two Mn^{2+} $3d$ orbitals, which are of the same type, added to the ZnO host. Clearly, in a more realistic calculation of FM correlations

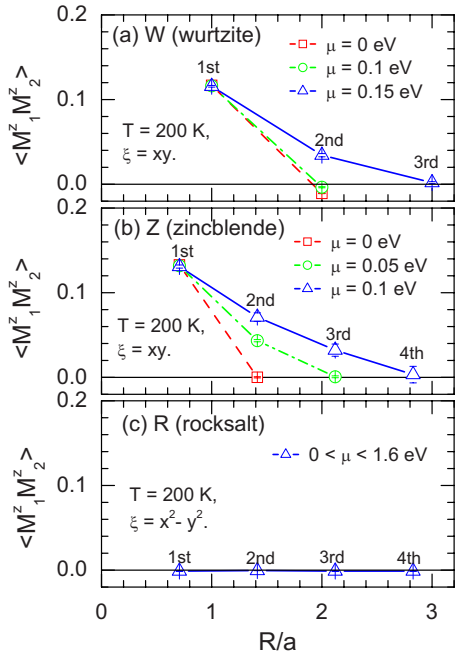

FIG. 4. (Color online) Impurity-impurity magnetic correlation function $\langle M_1^z M_2^z \rangle$ vs distance R/a for (a) the wurtzite, (b) zinc-blende, and (c) rocksalt structures. Here, each impurity site consists of a single Mn^{2+} $3d$ orbital. For the wurtzite and zinc-blende crystal structure, we have considered a $3d(xy)$ orbital at the impurity sites, while for the rocksalt case a $3d(x^2-y^2)$ orbital.

between the impurities, it would be necessary to consider the magnetic correlations between different types of $3d$ orbitals. However, our purpose in this paper is to investigate the role of the host electronic structure. In Fig. 4, the temperature $T=200$ K, $R=|R_1-R_2|$, and a is the lattice constant. In our chosen directions, the distance between the first-nearest-neighboring Mn^{2+} is a for the wurtzite structure, while it is $a\sqrt{2}/2$ for the zinc-blende and rocksalt structures. As shown in Fig. 4(a) for the wurtzite structure, the impurity spins exhibit FM correlations at $\mu=0.0$, but it is short range. By increasing μ to 0.15 eV, the range of the FM correlations becomes longer extending to the third-nearest-neighboring Mn^{2+}. Further increasing μ, the FM correlations becomes weaker. This is because the IBS of (Zn,Mn)O with wurtzite structure becomes occupied as μ changes above 0.15 eV, as seen in Fig. 3. For the zinc-blende structure, similar results are obtained. as shown in Fig. 4(b). The impurity spins exhibit FM correlations extending to the first-nearest-neighboring Mn^{2+} at $\mu=0.0$. Increasing μ to 0.1 eV, the FM correlations extend to the fourth-nearest-neighboring Mn^{2+}. Further increasing μ to above 0.1 eV, the FM correlations become weaker. This is because the IBS of (Zn,Mn)O with the zinc-blende structure becomes occupied as $\mu>0.1$ eV, as displayed in Fig. 3. We note that the compound (Zn,Mn)O with the zinc-blende structure seems to possess a longer range for the FM correlations than that with the wurtzite structure, while almost all existing experiments for ZnO are focused on the wurtzite structure. Not surprisingly, we have not observed magnetic correlations for the rocksalt structure in Fig. 4(c). This is because the position of IBS for (Zn,Mn)O with rocksalt structure is too deep, as seen in Fig. 3, thus the FM correlation range[22,23] is shorter than the first-nearest-neighbor distance.

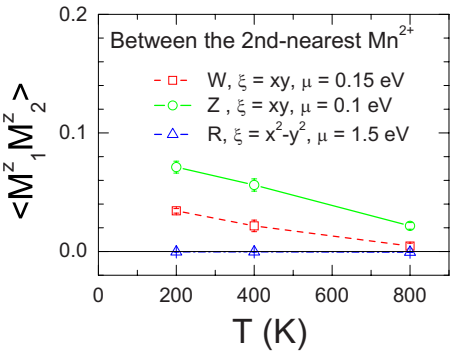

FIG. 5. (Color online) Impurity-impurity magnetic correlation function $\langle M_1^z M_2^z \rangle$ for second-nearest-neighbor impurity sites vs temperature T. Here, for the wurtzite and zinc-blende crystal structures, we have considered $3d(xy)$ orbitals, while for the rocksalt case $3d(x^2-y^2)$ orbitals.

We next study the temperature dependence of the FM correlations between the impurities in different crystal structures. Figure 5 displays the T dependence of $\langle M_1^z M_2^z \rangle$ for impurities which are second-nearest neighbors in wurtzite, zinc-blende, and rocksalt crystal structures. For wurtzite and zinc-blende structures, these calculations have been performed for the $3d(xy)$ orbitals, and for the rocksalt case they are for the $3d(x^2-y^2)$ orbital. In addition, for the wurtzite and zinc-blende structures, the chemical potential is taken as $\mu=0.15$ and 0.1 eV, respectively, where the IBS is unoccupied and the longest range of the FM correlations occurs, as shown in Fig. 4. The results for the rocksalt case are for $\mu=1.5$ eV, so that the IBS is unoccupied here also. We observe that as T decreases from 800 down to 200 K, the FM correlations grow for the wurtzite and zinc-blende structures. In this T range, the FM does not develop for the rocksalt case.

V. DISCUSSION

For the ZnO host with the rocksalt structure, it is useful to mention previous studies[30,38,39] that are related to the *indirect* energy gaps obtained with the sp^3 tight-binding calculation shown in Fig. 1(c). Using the HF method, Jaffe *et al.*[38] pointed out that for the rocksalt ZnO, the point symmetry in rocksalt structure does not allow for mixing between the Zn $3d$ orbitals and the O $2p$ orbitals at the Γ point, but mixing is allowed elsewhere in the Brillouin zone. Thus the valence band maximum shifts away form the Γ point so that the gap becomes indirect. As mentioned by Skinner and LaFemina in Ref. 30, where we follow their sp^3 tight-binding calculation for the ZnO host in present paper, this effect also exists even when the sp^3 tight-binding model does not *explicitly* include the Zn $3d$ orbitals because the Zn $3d$ character has been *implicitly* included in the hopping integrals through the tight-binding interpolation of the bulk *ab initio* pseudopotential bands[39] that Skinner and LaFemina used to derive them.

However, there also exist calculations for the rocksalt ZnO, which are based on the quasiparticle approach[40] and

the pseudopotential method,[41] yielding a *direct* energy gap at the Γ point. In order to understand the results observed for (Zn,Mn)O with the rocksalt structure, we have considered the case of MgO, whose crystal structure is also rocksalt but has a direct energy gap at the Γ point.[42] Using the tight-binding parameters given in Ref. 42, where the host basis consists of one *s* orbital for Mg^{2+} and three 2*p* orbitals for O^{2-}, we have calculated the *p-d* mixing for the compound (Mg,Mn)O as in the case for (Zn,Mn)O. We found that near the Γ point, the *p-d* mixing for (Mg,Mn)O with the rocksalt structure is also close to zero, where *d* stands for the five 3*d* orbitals. These results imply that the host compound with the rocksalt structure does not mix with the doped 3*d* orbitals at the Γ point regardless of whether there is a direct or indirect energy gap. In fact, this is generally true if the host with the rocksalt structure can be described using the sp^3 tight-binding approach. At the Γ point, because of the orthogonality of the *s* and *p* orbitals, we find that for a fixed band α, the coefficients $a_{\alpha p}$ in Eq. (2) have only one nonzero value, for example, *a*. Thus the *p-d* mixing at the Γ point has the form

$$V_\alpha(0) = a\sum_{\mathbf{n}} \langle \varphi_\xi(\mathbf{i})|H|\varphi_p(\mathbf{n})\rangle \equiv a\sum_{\mathbf{n}} E_{\xi,p}(\mathbf{i}-\mathbf{n}), \tag{6}$$

where ξ represents one of the five 3*d* orbitals and *p* denotes one of the *s*, p_x, p_y, and p_z orbitals. In addition, here, the summation is taken over the nearest neighbors, and $E_{\xi,p}(\mathbf{i}-\mathbf{n})$ is given using the notation of Slater and Koster,[32] which can be expressed in terms of the nonzero $(pd\sigma)$ and $(pd\pi)$, and the direction cosines *l*, *m*, and *n*. For the rocksalt structure, it can be shown that the value of $V_\alpha)(0)$, Eq. (6), vanishes for any ξ and *p* orbitals, when the summation is performed over the six nearest neighbors.

It is obvious that the magnetic correlations between the impurities depend on the position of the IBS, while the IBS is closely related the host band structure as well as the host-impurity mixing parameters. As mentioned above, for the rocksalt ZnO doped with magnetic impurities, the IBS will shift to the top of valence band if we decrease the values of the *p-d* mixing parameters $(pd\sigma)$ and $(pd\pi)$.

VI. SUMMARY AND CONCLUSIONS

In summary, we have studied the ferromagnetism for the compound (Zn,Mn)O with different crystal structures in the dilute impurity limit based on the Haldane–Anderson impurity model. The band structures of the ZnO host were calculated using the sp^3 tight-binding parameters from Ref. 30, and the *p-d* mixing parameters and the onsite Coulomb repulsion *U* were obtained from comparisons with the photoemission measurements on (Zn,Mn)O.[31] The QMC calculations show that the magnetic correlations between Mn^{2+} impurities in ZnO are strongly affected by the host crystal structure. For the wurtzite and zinc-blende structures, the FM correlations are found, and their range extends up to the third- or the fourth-nearest-neighbor sites at low temperatures. On the other hand, for the rocksalt structure, no magnetism has been found even between the nearest-neighbor impurities. In addition, only *p*-type ZnO doped with magnetic impurities is found to have ferromagnetism.

We think that to yield accurate predictions about DMS materials, the combining the band-calculation and QMC techniques is the first and crucial approach, where the strong electron correlation is exactly taken into account. In this paper, we combine the tight-binding calculations for the host band structure and the impurity-host hybridization with the QMC simulations. Our main purpose in this paper is to investigate the effect of the crystal structure on the IBS and the FM correlations for the ZnO host, thus our Haldane–Anderson model, which considers one of five *d* orbitals, is reasonably enough to explore the main properties of this effect. Thus in this paper, we ignored the multiorbital effect, where all of the impurity 3*d* orbitals are included with Hund couplings, because it is obviously another different effect.

It is generally agreed upon that the ferromagnetism in the DMS can be controlled by changing the type of the transition-metal impurities or the host semiconductor as well as the occupation of the IBS. The results presented in this paper suggest that the host crystal structure can also be used in the search for high-T_C ferromagnetism in DMS.

ACKNOWLEDGMENTS

This work was supported by the NAREGI Nanoscience Project and a Grant-in Aid for Scientific Research from the Ministry of Education, Culture, Sports, Science and Technology of Japan and NEDO. The authors thank the Supercomputer Center at the Institute for Solid State Physics, University of Tokyo, for the use of the facilities.

[1] H. Ohno, A. Shen, F. Matsukura, A. Oiwa, A. Endo, S. Katsumoto, and Y. Iye, Appl. Phys. Lett. **69**, 363 (1996); H. Ohno, Science **281**, 951 (1998).
[2] A. M. Nazmul, S. Sugahara, and M. Tanaka, Phys. Rev. B **67**, 241308(R) (2003).
[3] T. Jungwirth, K. Y. Wang, J. Masek, K. W. Edmonds, J. Konig, J. Sinova, M. Polini, N. A. Goncharuk, A. H. MacDonald, M. Sawicki, A. W. Rushforth, R. P. Campion, L. X. Zhao, C. T. Foxon, and B. L. Gallagher, Phys. Rev. B **72**, 165204 (2005).
[4] T. Dietl, H. Ohno, F. Matsukura, J. Cibert, and D. Ferrand, Science **287**, 1019 (2000).
[5] K. Sato and H. Katayama-Yoshida, Jpn. J. Appl. Phys. **40**, L334 (2001); K. Sato and H. Katayama-Yoshida, Physica E **10**, 251 (2001).
[6] P. Sharma, A. Gupta, K. V. Rao, F. J. Owens, R. Sharma, R. Ahuja, J. M. O. Guillen, R. Johansson, and G. A. Gehring, Nature Mater. **2**, 673 (2003).
[7] M. A. Garcia, M. L. Ruiz-Gonzalez, A. Quesada, J. L. Costa-Kramer, J. F. Fernandez, S. J. Khatib, A. Wennberg, A. C. Caballero, M. S. Martin-Gonzalez, M. Villegas, F. Briones, J. M. Gonzalez-Calbet, and A. Hernando, Phys. Rev. Lett. **94**, 217206 (2005).
[8] J. R. Neal, A. J. Behan, R. M. Ibrahim, H. J. Blythe, M. Ziese, A. M. Fox, and G. A. Gehring, Phys. Rev. Lett. **96**, 197208 (2006).
[9] D. F. Wang, S. Y. Park, Y. S. Lee, Y. P. Lee, J. C. Li, and C. Liu, J. Appl. Phys. **103**, 07D126 (2008).
[10] N. S. Norberg, K. R. Kittilstved, J. E. Amonette, R. K. Kukkadapu, D. A. Schwartz, and D. R. Gamelin, J. Am. Chem. Soc. **126**, 9387 (2004).
[11] S. W. Lim, M. C. Jeong, M. H. Ham, and J. M. Myoung, Jpn. J. Appl. Phys., Part 2 **43**, L280 (2004).
[12] M. Ivill, S. J. Pearton, D. P. Norton, J. Kelly, and A. F. Hebard, J. Appl. Phys. **97**, 053904 (2005).
[13] K. R. Kittilstved, N. S. Norberg, and D. R. Gamelin, Phys. Rev. Lett. **94**, 147209 (2005).
[14] K. R. Kittilstved, W. K. Liu, and D. R. Gamelin, Nature Mater. **5**, 291 (2006).
[15] M. Ivill, S. J. Pearton, Y. W. Heo, J. Kelly, A. F. Hebard, and D. P. Norton, J. Appl. Phys. **101**, 123909 (2007).
[16] S. W. Jung, S. J. An, G. C. Yi, C. U. Jung, S. I. Lee, and S. Cho, Appl. Phys. Lett. **80**, 4561 (2002).
[17] G. Lawes, A. S. Risbud, A. P. Ramirez, and R. Seshadri, Phys. Rev. B **71**,

045201 (2005).
[18]T. Fukumura, Z. Jin, M. Kawasaki, T. Shono, T. Hasegawa, S. Koshihara, and H. Koinuma, Appl. Phys. Lett. **78**, 958 (2001).
[19]A. Tiwari, C. Jin, A. Kvit, D. Kumar, J. F. Muth, and J. Narayan, Solid State Commun. **121**, 371 (2002).
[20]S. Venkataraj, N. Ohashi, I. Sakaguchi, Y. Adachi, T. Ohgaki, H. Ryoken, and H. Haneda, J. Appl. Phys. **102**, 014905 (2007).
[21]F. D. M. Haldane and P. W. Anderson, Phys. Rev. B **13**, 2553 (1976).
[22]M. Ichimura, K. Tanikawa, S. Takahashi, G. Baskaran, and S. Maekawa, *Foundations of Quantum Mechanics in the Light of New Technology*, edited by S. Ishioka and K. Fujikawa, (World Scientific, Singapore, 2006), pp. 183–186.
[23]N. Bulut, K. Tanikawa, S. Takahashi, and S. Maekawa, Phys. Rev. B **76**, 045220 (2007).
[24]K. Sato and H. Katayama-Yoshida, Phys. Status Solidi B **229**, 673 (2002).
[25]H. Katayama-Yoshida and K. Sato, Physica B **327**, 337 (2003).
[26]E. C. Lee and K. J. Chang, Phys. Rev. B **69**, 085205 (2004).
[27]N. A. Spaldin, Phys. Rev. B **69**, 125201 (2004).
[28]P. M. Krstajić, V. A. Ivanov, F. M. Peeters, V. Fleurov, and K. Kikoin, Europhys. Lett. **61**, 235 (2003).
[29]J. Inoue, S. Nonoyama, and H. Itoh, Phys. Rev. Lett. **85**, 4610 (2000).
[30]A. J. Skinner and J. P. LaFemina, Phys. Rev. B **45**, 3557 (1992).
[31]T. Mizokawa, T. Nambu, A. Fujimori, T. Fukumura, and M. Kawasaki, Phys. Rev. B **65**, 085209 (2002).
[32]J. C. Slater and G. F. Koster, Phys. Rev. **94**, 1498 (1954).
[33]W. Harrison, *Electronic Structure and the Properties of Solids* (Freeman, San Francisco, 1980).
[34]S. Maekawa, T. Tohyama, S. E. Barnes, S. Ishihara, W. Koshibae, and G. Khaliulin, *Physics of Transition Metal Oxides*, Solid-State Sciences, Vol. 144 (Springer, New York, 2004).
[35]J. E. Hirsch and R. M. Fye, Phys. Rev. Lett. **56**, 2521 (1986).
[36]Y. Tomoda, N. Bulut, and S. Maekawa, arXiv:0806.0095.
[37]J. W. Quilty, A. Shibata, J. Y. Son, K. Takubo, T. Mizokawa, H. Toyosaki, T. Fukumura, and M. Kawasaki, Phys. Rev. Lett. **96**, 027202 (2006).
[38]J. E. Jaffe, R. Pandey, and A. B. Kunz, Phys. Rev. B **43**, 14030 (1991).
[39]J. R. Chelikowsky, Solid State Commun. **22**, 351 (1977).
[40]H. Q. Ni, Y. F. Lu, and Z. M. Ren, J. Appl. Phys. **91**, 1339 (2002).
[41]D. Fritsch, H. Schmidt, and M. Grundmann, Appl. Phys. Lett. **88**, 134104 (2006).
[42]V. C. Lee and H. S. Wong, J. Phys. Soc. Jpn. **45**, 895 (1976).